



Polyhydroquinoline nanoaggregates: A dual fluorescent probe for detection of 2,4,6-trinitrophenol and chromium (VI)

Jigyasa^a, Deepak Kumar^a, Priya Arora^a, Harminder Singh^b, Jaspreet Kaur Rajput^{a,*}

^a Department of Chemistry, Dr. B R Ambedkar National Institute of Technology, Jalandhar 144011, Punjab, India

^b DAV University, Jalandhar 144001, Punjab, India

ARTICLE INFO

Article history:

Received 11 October 2019

Received in revised form 7 January 2020

Accepted 20 January 2020

Available online 21 January 2020

Keywords:

Fluorescent nano-aggregates

Polyhydroquinolines

Test-strips

Dual detection probe

AIEE

ABSTRACT

Fluorescent polyhydroquinoline (PHQ) derivative was fabricated utilizing one-pot engineered course. The PHQ derivative indicated aggregation induced emission enhancement (AIEE) with arrangement of nanoaggregates of size 11–13 nm in 95% watery DMF medium. The fluorescence emission of PHQ nanoaggregates was extinguished by including TNP and Cr (VI). They indicated prevalent fluorescence quenching towards both TNP and Cr (VI) over other meddling nitro-compounds and metal particles. In light of results got we presumed that both photo-induced fluorescence quenching of PHQ nanoaggregates by TNP, while Inner Filter Effect (IFE) was in charge of fluorescence quenching of PHQ nanoaggregates by Cr (VI). The PHQ nanoaggregates empowered identification of TNP and Cr (VI) down to 0.66 μM (TNP) and 0.28 μM (Cr (VI)). The use of PHQ nanoaggregates were reached out for location of TNP and Cr (VI) in genuine water tests.

© 2020 Published by Elsevier B.V.

1. Introduction

Ecological security concerns have arrived at alarmingly abnormal states inferable from nonstop unreasonable human exercises. The unregulated use and disposal of hazardous compounds have brought about negative impacts on the earth. Substantial metal particles and nitroaromatic compounds (NACs) fall into the classification of hazardous compounds that posture potential danger to human wellbeing and environment [1]. NACs, for example, trinitrotoluene (TNT), 2,4,6-trinitrophenol (TNP), 2,4-dinitrotoluene (2,4-DNT), 2,4-dinitrophenol (2,4-DNP), 4-nitrotoluene (4-NT), nitrobenzene (NB), and so on are arranged under mixes with prospective danger of fear based oppression and natural security in various nations [2]. Among different NACs, TNP otherwise called picric acid, is viewed as the most threatening as it shows high explosive velocity [3] and low wellbeing coefficient [4]. Likewise, TNP has higher water dissolvability than TNT [5], along these lines genuinely contaminating ground water, soil and air [1]. TNP is broadly utilized in rocket powers, firecrackers, dyes [6], matches, pharmaceutical, and leather businesses [2]. The persistent ingestion of TNP may cause skin/eye bothering, sickness, dazedness, spewing, and stomach torment [4,7]. There are reports where TNP has been utilized by terrorist groups for blasts in several areas [8].

Then again, chromium (VI) is a famous lethal substantial metal that aggravates the biological system [9]. Among the two watery stable

conditions of chromium, Cr (III) and Cr (VI), Cr (VI) is known to have cancer-causing nature and mutagenicity towards living life forms [10]. It is broadly utilized in metallurgy, leather tanning, dyeing and catalysis industry [11]. The most extreme degree of Cr (VI) in drinking water, allowable by World Health Organization is 1 μM [12]. In any case, shockingly because of unregulated mechanical waste release into the inland surface water, the substantial metal contamination is viewed as genuine risk in numerous pieces of world, particularly the developing nations [13]. Globally the defilement of drinking water supply by Cr (VI) is of extraordinary concern [14]. Ingestion of Cr (VI) polluted water can cause queasiness, liver and kidney harm [15] and hemolysis [16].

There are different very much established scientific procedures for location of Cr (VI) that includes electrochemistry [17], atomic absorption spectroscopy [18], inductively coupled plasma mass spectrum (ICP-MS) [19,20], and high performance liquid chromatography (HPLC) [21,22]. Similarly numerous analytical methods have been reported for monitoring TNP content in common matrix, including ion chromatography [23], electrochemical techniques [23,24], ion-mobility spectrometry [25], Raman spectroscopy [26], and so forth have been reported. Despite the fact that these strategies offer high affectability however experience the ill effects of complicated instrumentation, tedious and advanced pretreatment, subsequently restricting their utilization for on location identification [27,28]. Among every one of these strategies the fluorescence based chemosensors are the one that have advanced a ton inferable from on location appropriateness, high affectability, cost viability and accessible instrument prerequisite [10,29]. Considering the advantages of fluorescent-based touchy

* Corresponding author.

E-mail address: rajputj@nitj.ac.in (J.K. Rajput).

sensors, a marketed sensor FidoXT have been made [30]. It involves amplifying fluorescence polymers that empowered location of military-grade mixes utilized in hand crafted explosives and IED's, incorporating PETN in parts per quadrillion (ppq) [31,32]. There are different fluorescent based sensors like nanosheets [33,34], nanoaggregates [35], conjugated polymers [36], quantum dots [37], carbon dots [38], metal organic frameworks [39,40] answered to identify and measure different metal particles and NACs. There are various fluorescent sensors that permit location of metal particles or NACs in non-aqueous medium; anyway their appropriateness is interfered with when connected in watery medium [41]. This is on the grounds that most fluorescent mixes show aggregation caused quenching (ACQ) in aqueous medium. It's a phenomenon wherein a fluorophore show debilitated fluorescence in aqueous medium attributable to solid collection actuated π - π stacking by hydrophobic aromatic backbone [35]. Over the previous decades there are rich reports of accumulation induced emission (AIE) or aggregation induced emission enhancement (AIEE) materials, which demonstrate no or frail fluorescence in arrangement yet show solid luminescence in the aggregated state [42]. Organic molecules such as pentacenequinone [43], naphthalimide [44], α -cyanostilbene [42], tetraphenylethylene [45], siloles, arylethene derivatives that emit strongly in their aggregated or solid state have been reported [43].

In this, we have synthesized a polyhydroquinoline subordinate by an effortless one-pot course which framed fluorescent nanoaggregates in blended fluid media. Polyhydroquinoline are significant structural motif in view of biological as well as medicinal applications. It acts like donor-acceptor framework where the heading of charge movement is from the benzene ring towards the quinoline ring [46]. As far as we could possibly know it's the primary report where fluorescent nanoaggregates of polyhydroquinolines are utilized for double identification of Cr (VI) and TNP.

2. Experimental section

2.1. Chemicals and reagents

Dimedone or 5,5-dimethyl-1,3-cyclohexanedione (99%), ethyl acetoacetate (98%), *N,N*-dimethylformamide from Loba Chemie; 3-methoxybenzaldehyde (98%) and ammonium acetate (98%) from Avra Synthesis. Milli-Q water was utilized all through the experimental procedure.

2.2. Instrumentation

Fourier Transform IR (FTIR) spectra were recorded on Agilent Cary 600 in the range 400–4000 cm^{-1} . ^1H Nuclear Magnetic Resonance spectra were recorded at 400 MHz with the guide of Advance 400 spectrophotometer, utilizing tetramethylsilane as the internal standard and CDCl_3 as a dissolvable. The following abbreviations were utilized to depict peak parting designs: s = singlet, d = doublet, t = triplet, br = broad, and m = multiplet. ESI-MS spectra were recorded on a XEVO G2-XS QTOF spectrometer. Melting points were recorded by Gallenkamp apparatus and were uncorrected. The nanomorphology of

the fluorescent nanoaggregates was studied using high resolution transmission electron microscope (HR-TEM) of make Jeol/JEM 2100. The UV spectra were recorded on Agilent Technologies Cary arrangement UV-vis spectrophotometer with a quartz cuvette (way length, 1 cm). The fluorescence spectra were recorded on Agilent Cary Eclipse spectrofluorimeter. The cut width for fluorescence test was at 5 nm (excitation) and 5 nm (emission) for all fluorescence considers. DELTADP-auto Dip coater was utilized for getting ready visual test strips. Time-Resolved fluorescence studies were performed on Horiba Jobin Yvon Time-Resolved Fluorescence Spectrometer instrument utilizing time-correlated single photon counting (TPSPC) strategy. The cyclic voltammetry was performed utilizing CH instruments (USA), CHI-600E.

2.3. Synthesis of chemosensor (PHQ)

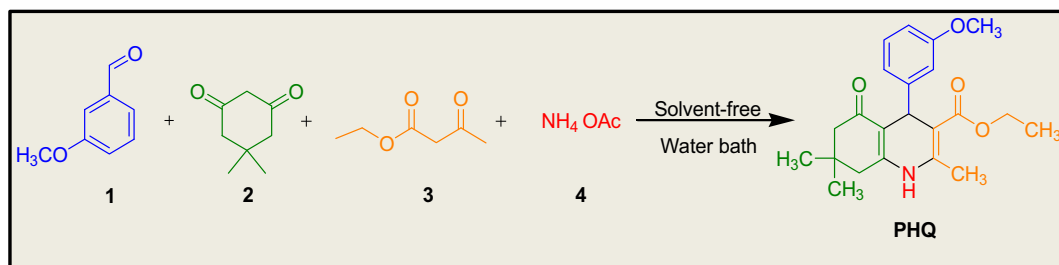
The compound (PHQ) was synthesized through a one-pot multi-component reaction as depicted in Scheme 1. A blend of 3-methoxybenzaldehyde (1 mmol), ethyl acetoacetate (1 mmol), dimedone or 5,5-dimethyl-1,3-cyclohexanedione (1 mmol), ammonium acetate (1 mmol) was warmed in on a preheated water bath for 30 min. The advancement of the reaction was monitored by TLC. After completion of the reaction, the mixture was dissolved in hot EtOH. It was later cooled to room temperature. The solid product so acquired was filtered, followed by washing with distilled water. The pure product was then acquired through recrystallization of impure product from EtOH. The formation of product was affirmed by FT-IR, ^1H NMR, ESI-MS and ^{13}C NMR (Supporting Information Figs. ES1–ES3).

2.4. Compound PHQ: ethyl-1,4,7,8-tetrahydro-2,7,7,4-(3-methoxyphenyl)-5-(6H)-oxoquinolin-3-carboxylate

Light yellow solid; yield: 85.03%; M.p. 188–190 $^{\circ}\text{C}$; FT-IR (cm^{-1}): 3306, 3217, 3083, 2948, 2107, 1696, 1607, 1472, 1383, 1267, 1204, 1142, 1026, 864, 766, 685, 578, and 507 cm^{-1} ; ^1H NMR (400 MHz, CDCl_3 , δ ppm) 0.91 (s, 3H, CH_3), 1.06 (s, 3H, CH_3), 1.21 (t, 3H, OCH_2CH_3), 2.18–2.29 (m, 4H, $2\times\text{CH}_2$), 2.36 (s, 3H, $=\text{C}-\text{CH}_3$), 3.74 (s, 3H, OCH_3), 4.06 (q, 2H, OCH_2CH_3), 5.04 (s, 1H, Ar—C—H), 5.93 (s, 1H, N—H), 6.65 (d, Ar—H), 6.86–7.08 (m, 2H, Ar—H), 7.26 (s, 1H, Ar—H), and 7.26 (s, 1H, Ar—H). ESI MS (m/z): calculated for $\text{C}_{22}\text{H}_{27}\text{NO}_4 = 369.19$; found 370.21 [$M + 1$]. Anal. calcd. for $\text{C}_{22}\text{H}_{27}\text{NO}_4$: C, 71.52; H, 7.37; and N, 3.79. Found: C, 71.62; H, 7.99; and N, 3.54.

2.5. Synthesis of fluorescent nanoaggregates

The nanoaggregates of PHQ were set up by re-precipitation technique. In a typical procedure, fitting measure of DMF and water was utilized to get blends with water part of 0–99%. The stock arrangement of PHQ was set up in DMF (10^{-3} M). An aliquot of this stock arrangement was moved to the ceaselessly mixed DMF:water blends (0–99%) to get 30 μM of PHQ in DMF:water blends 0–99%. The so formed nanoaggregates were permitted to remain at room temperature for 30 min. The subsequent blends were characterized through spectral investigation.



Scheme 1. One-pot route for the synthesis of compound PHQ.

2.6. Fluorescence quenching titrations

A 2.5 ml solution of PHQ nanoaggregates (30 μM in 95% aqueous DMF) was titrated with increasing concentrations of TNP and Cr (VI) (0–170 μM). The change in emission spectra of PHQ nanoaggregates was analyzed after incubation of 10 min (TNP) and 15 min (Cr (VI)). The emission spectra of each sample were estimated upon excitation at 370 nm. For selectivity investigations of NACs solution of 10^{-3} M of: phenol, 2-nitrotoluene, 1,3-dinitrobenzene, nitromethane, nitrobenzene and TNP were prepared and diluted to required concentrations. Similarly aqueous solution of metal ions: Fe^{2+} , Hg^{2+} , Cu^{2+} , Cs^+ , Cd^{2+} , Zn^{2+} , Pb^{2+} , Sn^{2+} , Co^{2+} , NO_3^- , SCN^- , N_3^- , AcO^- and Cr^{6+} were set up for selectivity examines.

2.7. Fluorescence quantum yield

Fluorescence quantum yield (ϕ) of PHQ was calculated with respect to quinine sulphate (QS) in 0.1 M H_2SO_4 as per following formulae:

$$\phi_s = \phi_R \times \frac{I_s \times A_R \times \eta_s^2}{I_R \times A_S \times \eta_R^2} \quad (1)$$

where ϕ_s = quantum yield of sample (PHQ); ϕ_R = quantum yield of reference (0.54); I_s = Integrated fluorescence intensity of sample; I_R = Integrated fluorescence intensity of reference; A_R = absorbance of the reference; A_S = absorbance of the sample; η_s = refractive index of sample; η_R = refractive index of reference.

2.8. Cyclic voltammetry (CV) experiments

The cyclic voltammetry was performed using tetrabutylammonium fluoride as a supporting electrolyte, glassy carbon electrode as a working electrode, platinum as a counter electrode and Ag/AgCl as a reference electrode. The scan rate was 50 mV/s. The LUMO energy level was calculated by applying the equation: $E_{\text{LUMO}} = -(4.8 - E_{1/2\text{Fc}^+/\text{Fc}} + E_{\text{red onset}})$, where $E_{\text{red onset}}$ is onset reduction potential relative to Ag/AgCl reference electrode. The HOMO energy level was calculated by applying the equation: $E_{\text{HOMO}} = E_{\text{LUMO}} - E_{\text{g, optical}}$, where $E_{\text{g, optical}}$ is optical band gap, estimated from the absorption edge ($E_{\text{g, optical}} (\text{eV}) = 1240 / \lambda_{\text{onset}}$) [47–49].

2.9. Visual detection of TNP using luminescent test strips

TNP can pollute compartments, subjects, attire and different materials by leaving its follows during assembling of fireworks, transportation and handling. Cr (VI), other notorious sully water bodies through leakage from tanning and metallurgy industry. Henceforth their on location identification is highly desirable. To empower versatility and minimal effort on location identification, fluorescent test strips were manufactured. The Whatman filter paper was covered in PHQ nanoaggregates arrangement (95% watery DMF) through the guide of DELTADP-auto Dip coater. The coater was worked at a down speed of 150 mm, delay time 2 s, tank time 15 s, and number of cycles 2. The test strips were later dried in vacuum oven. TNP and Cr (VI) solutions of varied concentrations were spotted on dried test strips. The strips were then seen under 365 nm UV light and pictures were taken utilizing advanced camera.

3. Results and discussion

3.1. Design and synthesis of chemosensor

The compound PHQ was synthesized through an advantageous one-pot course. The so obtained chemosensor was well described by FTIR, ^1H NMR, Fluorescence and UV examination. PHQ derivative filled in as proficient chemosensor for identification of TNP and Cr (VI) in 95% fluid

medium. The PHQ nanoaggregates indicated considerable fluorescence quantum yield of 0.042.

3.2. Photophysical properties of fluorescent nanoaggregates

The UV–Vis absorption spectrum of PHQ show absorption bands at 293 and 358 nm in DMF that could be expected to π – π^* changes. So as to think about the wonders of AIEE appeared by PHQ derivative, UV–Vis and fluorescence studies were performed [46]. The UV–Vis and fluorescent spectrum of PHQ derivative were recorded with various volume part of water (f_w), while keeping its concentration at 30 μM . The UV–Vis spectral pattern of PHQ remained ideal up to 60% f_w , with $\lambda_{\text{max. abs.}}$ at 364 nm (Fig. 1a). Further addition of over 60% f_w in DMF arrangement of PHQ absorbance band indicated stamped changes. A fast bathochromic move is seen alongside phantom widening and level off tailing. The emerging of level-off tail in UV–Vis range (Fig. 1b) estimated the presence of Mie scattering brought about by aggregated particles [50,51]. The increase in polarity of the medium results in feeble π – π stacking among nanoaggregates which further prompts extension of viable conjugation in them.

The fluorescent profile of PHQ in differed DMF:water portions were likewise researched. In unadulterated DMF, PHQ showed frail fluorescence discharge centered at 423 nm on excitation at 370 nm. Strangely on expanding the f_w to 60% in DMF checked elevate in fluorescence emission alongside bathochromic move of 23 nm was observed (Fig. 1c). Later on expanding the f_w from 60% to 95% a little increase in fluorescence power was watched. Further expansion of 99% f_w to DMF arrangement of PHQ brought about abatement in fluorescence power (Fig. 1d). This perception is generally seen in atoms indicating AIEE properties. Wherein after arrangement of aggregates, atoms appended distinctly to the outside of collected particles discharge light and in this manner add to overall drop in original fluorescence of the complete aggregated structure.

To better comprehend the marvels of AIEE, fluorescence lifetime study was likewise explored. The augmentation in fluorescence lifetime of nanoaggregates of organic compound in contrast with that of unadulterated organic compound affirmed the development of nanoaggregates (Fig. ES4). A deferred fluorescence decay time uncovered that the non-radiative procedures of the electronically energized state of PHQ are diminished attributable to generation of molecular aggregation [52].

The consequences of UV–Vis absorption, fluorescence emission and time-resolved fluorescence study unarguably supported the presence of AIEE wonders in PHQ derivative. The aggregation of molecules totally restricted the intramolecular rotation (RIR). There are two sorts of aggregates: H-type and J-type depending on blue and red shift in absorption/emission, respectively. In this on increasing f_w in DMF, PHQ derivatives showed J-type aggregation in which absorption and emission bands are red-shifted which are intense and narrow contrasted with monomer [53,54]. The HR-TEM examination further affirmed the arrangement of requested nanoaggregates. The nanoaggregates of size of 11–13 nm were obtained. The nanoparticles within the aggregate were spherical in morphology (Fig. 2).

The optical stability of the nanoaggregates was additionally assessed by setting it under a constant 365 nm UV light brightening. The change in fluorescence emission was determined at interim of 20 min inside restricted light time of 60 min. The fluorescence of the chemosensor didn't weaken much during consistent light, which demonstrates positive optical stability of the PHQ nanoaggregates (Fig. ES6).

3.3. Fluorescent detection of TNP by PHQ nanoaggregates

To investigate the use of PHQ nanoaggregates for recognition of TNP, fluorescence quenching titrations were carried out. The gradual addition of TNP was done and change in emission profile was analyzed. The fluorescence emission of PHQ was steadily extinguished up to

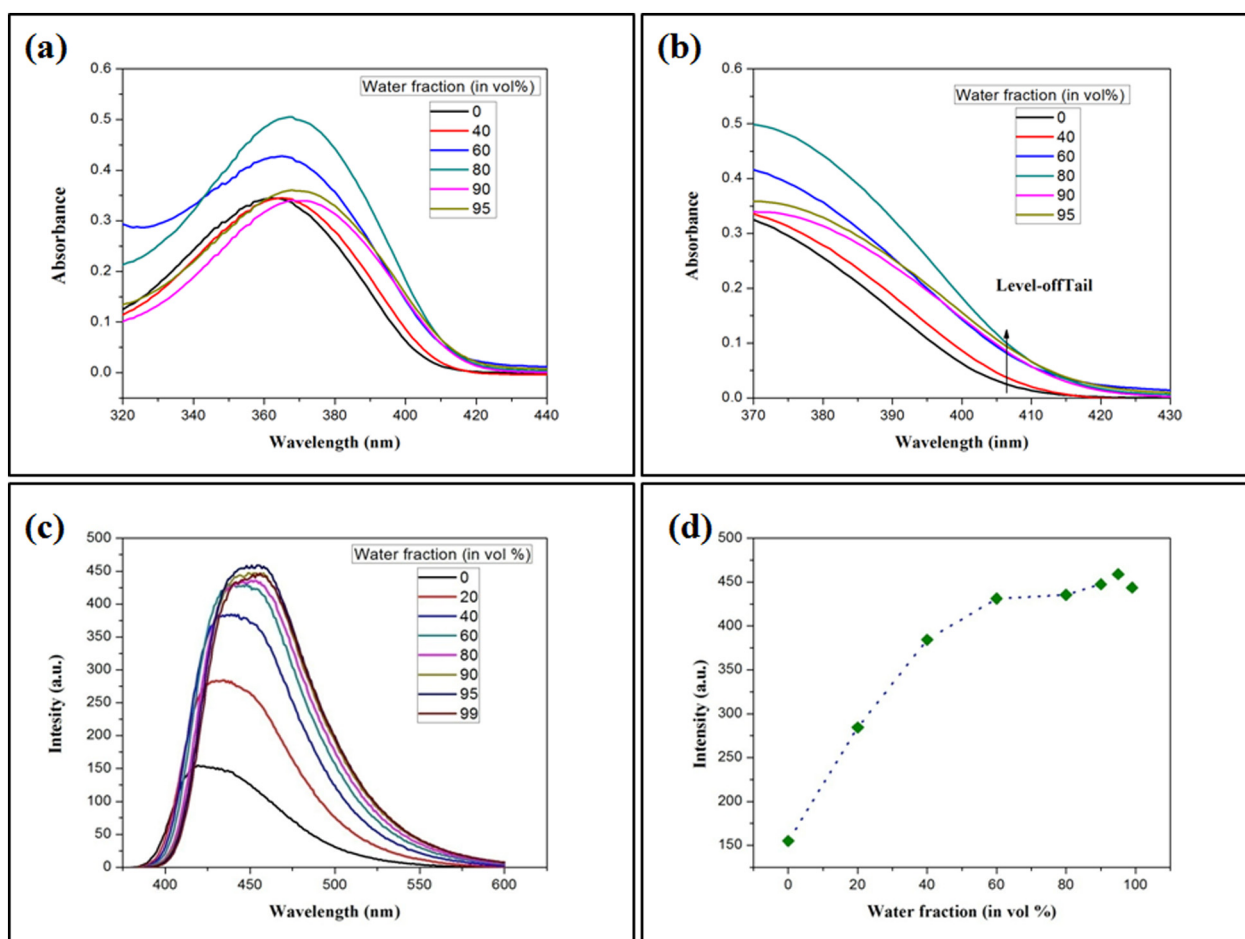


Fig. 1. Changes in UV-Visible (a & b) and fluorescence profile (c & d) of PHQ in DMF-water mixtures with different water volume fractions.

addition of 170 μM of TNP alongside diminishing of blue emission of fluorescent nanoaggregates. The adjustment in fluorescence profile was analyzed utilizing Stern-Volmer plot:

$$F_0/F = K_{SV} [A] + 1 \quad (2)$$

where F_0 and F are fluorescence intensity of PHQ nanoaggregates in presence and absence of TNP, $[A]$ is the concentration of analyte and

K_{SV} is Stern-Volmer constant. The S-V plot showed linear relationship with the TNP concentration in the range of 0–70 μM (Fig. 3c). As shown in Fig. 3b the S-V plot deviated from linearity bending in upward direction at high concentration of TNP. This linearity at low concentration of TNP is ascribed to static quenching whereas the upward bending at high concentration of TNP can be presumably due to dynamic quenching. The regression equation was $F_0/F = 0.016x_{(\text{TNP})} + 1.123$ with the correlation coefficient (r) of 0.987 (Fig. 3(c)), and the detection

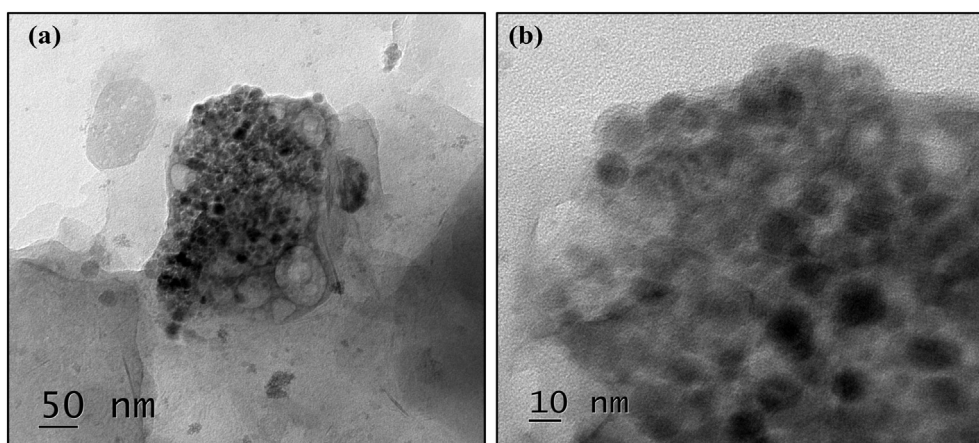


Fig. 2. HR-TEM images of PHQ nanoaggregates.

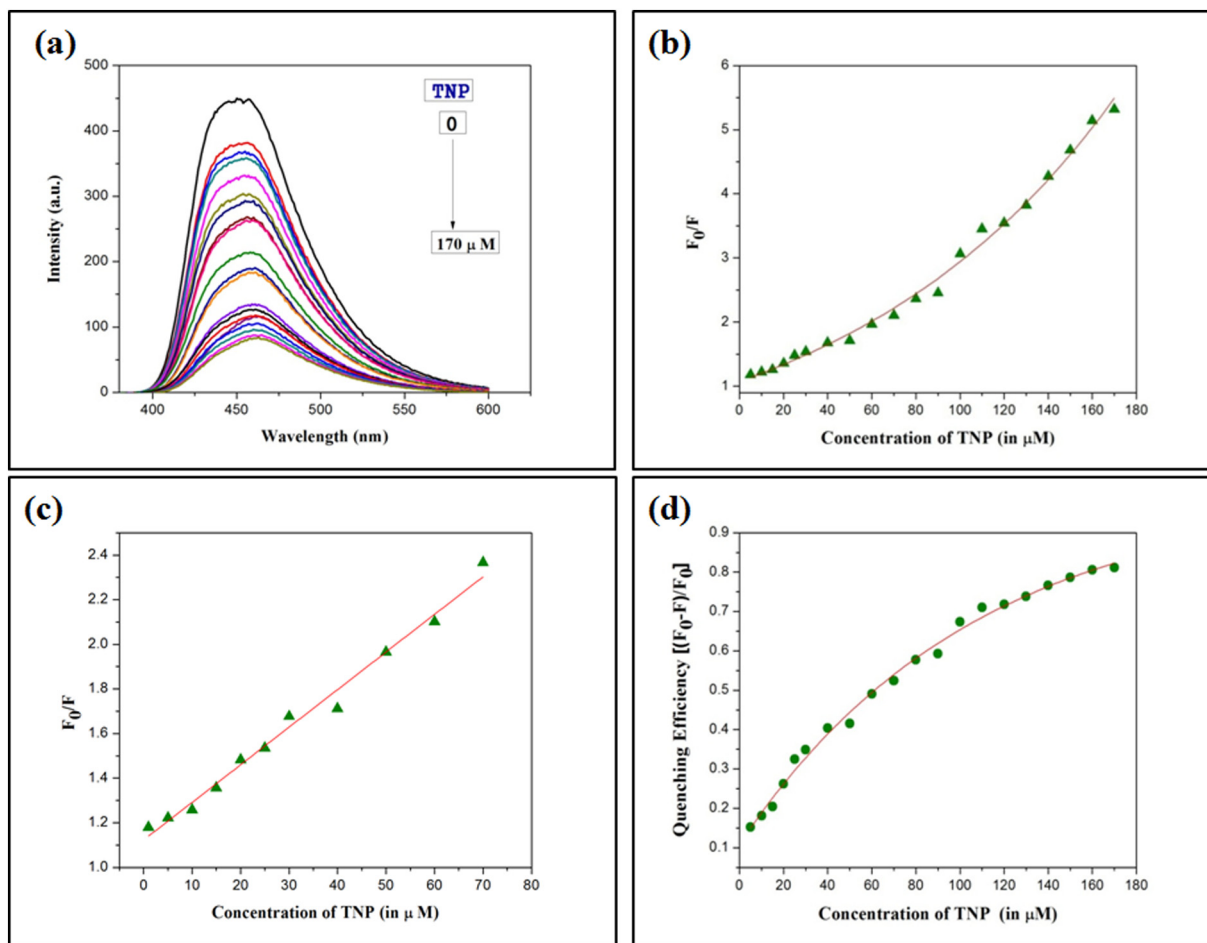


Fig. 3. (a) Fluorescence quenching of PHQ aggregates on addition of different concentration of TNP. (b) Stern-Volmer plot for fluorescence quenching of PHQ nanoaggregates by TNP. (c) Linearity in Stern-Volmer plot at low concentration of TNP. (d) Quenching response of PHQ nanoaggregates towards TNP.

limit was calculated to be 0.66 μM . To further study the fluorescence quenching of PHQ towards TNP, a plot of $(F_0 - F) / F_0$ versus concentration of TNP (Fig. 3d), was analyzed. It was observed that quenching efficiency of PHQ towards TNP increased drastically at low concentration of TNP and attained a leveled off position at high concentration of TNP (above 100 μM). To comprehend the binding stoichiometry between PHQ and TNP, Job's continuous variation method was employed. The concentration of PHQ and TNP were varied, while the sum of the two concentrations was kept constant at 10 μM . Maximum change was observed at 0.33 mol ratio of $[\text{PHQ}] / ([\text{PHQ}] + [\text{TNP}])$ (Fig. ES5 (a)), thus indicating 1:2 complexation between PHQ and TNP. The association of PHQ-TNP complex was determined using the Benesi-Hildebrand equation. In case of 1:2 stoichiometric complex formations a modified equation was used:

$$1/(F_0 - F_i) = 1/\{K_a * (F_0 - F_{\min}) * [\text{TNP}]^2\} + 1/(F_0 - F_{\min}) \quad (3)$$

Herein, F_0 , F_i and F_{\min} are the fluorescence intensity of PHQ at nm in the absence of TNP, at given concentration of TNP and with the addition of excess amount of TNP, respectively. K_a is the binding constant or association constant. The linear fitting of Benesi-Hildebrand plot strongly supported the formation of 1:2 binding stoichiometry between PHQ and TNP (Fig. ES5 (b)). From the plot of $[1 / (F_0 - F_i)]$ versus $[\text{TNP}]^{-2}$, the value of K_a is found to be $4.4 \times 10^4 \text{ M}^{-2}$, which suggested good complexation between TNP and PHQ.

3.4. Fluorescent detection of Cr (VI) by PHQ nanoaggregates

Like TNP, introduction of Cr (VI) into the solution of chemosensor resulted into marked quenching in the fluorescence intensity of the chemosensor (Fig. 4a). The quenching impact of the quencher Cr (VI) on fluorescence emission of PHQ nanoaggregates was additionally dictated by Stern-Volmer condition (Eq. 2). A plot of F_0/F versus $[\text{Cr (VI)}]$ (Fig. 4c) indicated linearity at low concentration, while at high centralization of Cr (VI) the plot veered off from linearity the upward way (Fig. 4b). The regression equation was $F_0/F = 0.016x_{(\text{TNP})} + 1.006$ with the relationship coefficient (r) of 0.975 (Fig. 3(c)), and detection limit was calculated to be 0.28 μM . The fluorescence intensity of the sensing probe had no noteworthy change within the sight of different particles (Fig. 8a). This demonstrated that the chemosensor showed high selectivity towards identification of Cr (VI). To further understand the quenching behavior of sensing probe towards Cr (VI), a plot of $(F_0 - F) / F_0$ versus varied concentration of TNP (Fig. 4d), was analyzed. It was seen that quenching effectiveness expanded quickly at low convergence of Cr (VI), though at high concentration (over 90 μM) a leveled off position was achieved.

3.5. Fluorescence intensity time response study & real sample analysis

For structuring of a productive sensor its reaction time ought to be extremely expeditious towards the analyte. The impact of response time on the relative fluorescence intensity of the PHQ nanoaggregates

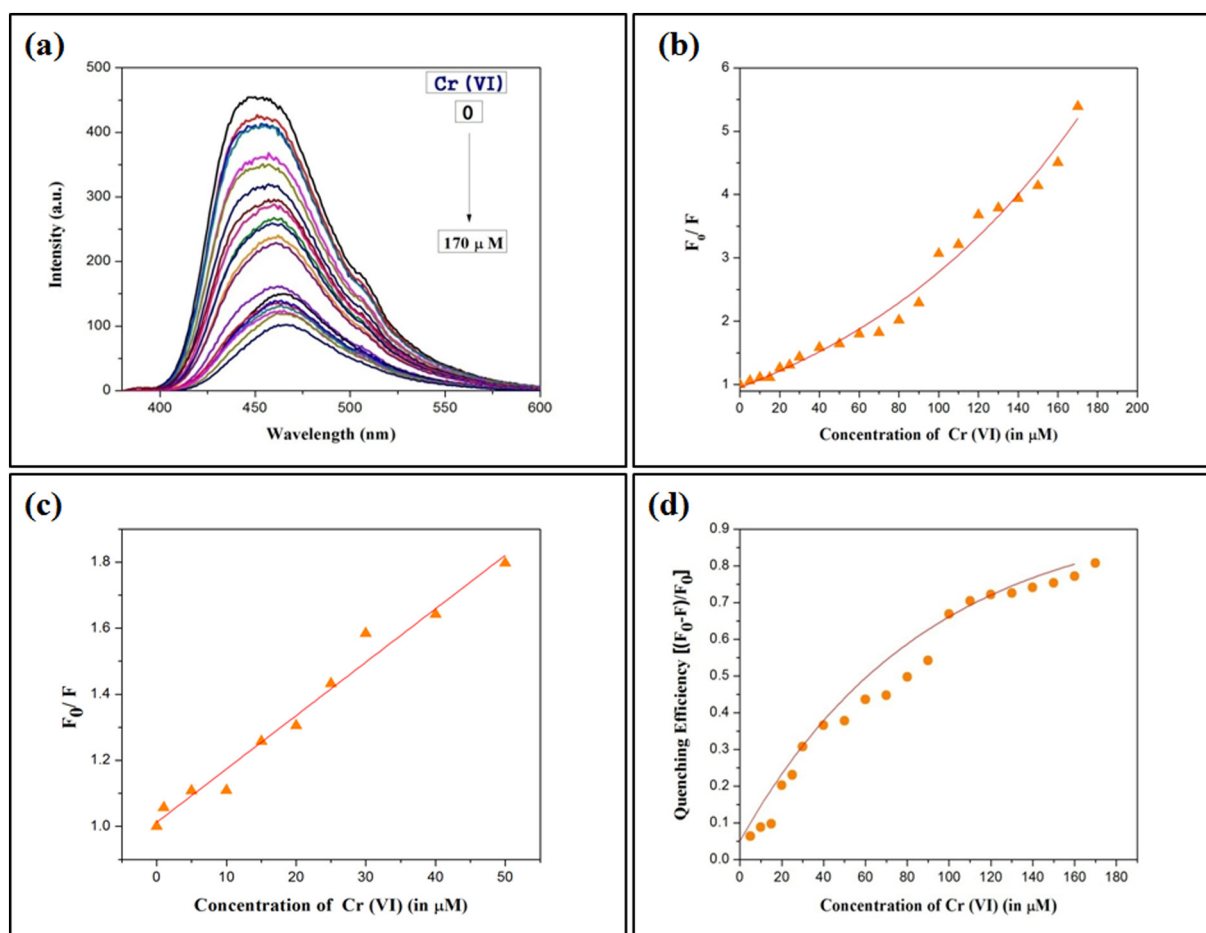


Fig. 4. (a) Fluorescence quenching of PHQ aggregates on addition of different concentration of Cr (VI). (b) Stern-Volmer plot for fluorescence quenching of PHQ nanoaggregates by Cr (VI). (c) Linearity in Stern-Volmer plot at low concentration of Cr (VI). (d) Quenching response of PHQ nanoaggregates towards Cr (VI).

in the presence of Cr (VI) and TNP was researched. As appeared in Fig. 5, the value of F_0/F increments quickly at first (0–10 min for TNP and 0–15 min for Cr (VI)) while after 10 min (TNP) and 15 min (Cr (VI)) no further particular change was observed. Subsequently 10 min and 15 min were picked as ideal incubation time for location of TNP and Cr (VI).

The practicality of the proposed sensing probe for discovery of Cr (VI) and TNP in genuine water tests was researched. Tap water and

lake water samples were spiked with TNP (30 μM) and Cr (VI) (30 μM). The quenching effectiveness of the sensing probe towards recognition of Cr (VI) and TNP in real samples was determined as shown in Fig. 6. The outcomes proposed that the prepared PHQ sensor test showed promising potential for checking Cr (VI) and TNP in real water samples (Table 1).

For recovery experiments samples (tap and pond water) were spiked with different concentrations of TNP and Cr (VI) and then the

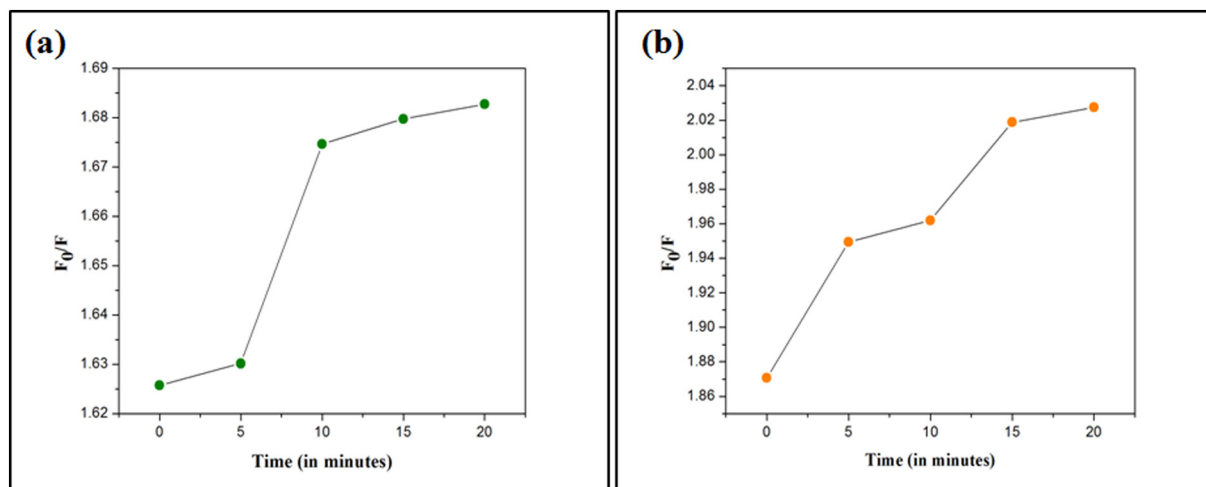


Fig. 5. Time-dependent fluorescence ratio (F_0/F) changes of PHQ nanoaggregates towards (a) TNP and (b) Cr (VI).

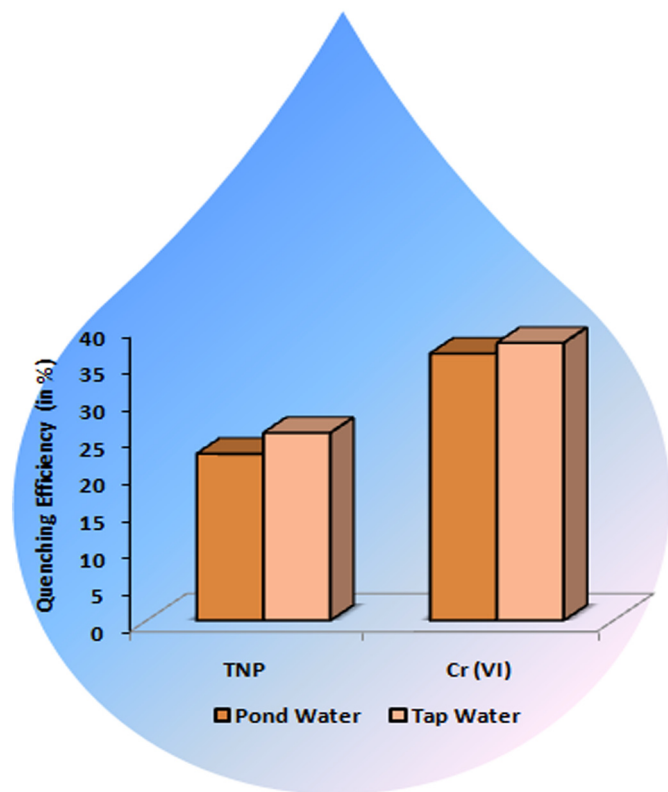


Fig. 6. Quenching efficiency of PHQ nanoaggregates towards TNP and Cr (VI) in real samples.

Table 1
Determination of TNP/Cr (VI) in water samples using PHQ nanoaggregates.

Sample	Amount of sample added (μM)	Amount of sample found (μM)	Recovery (%)	
TNP	Tap water	20	18.9	94.5
	Pond water	20	17.1	85.5
Chromium	Tap water	40	45.5	113.7
	Pond water	40	43.3	108.2

spiked water samples were tested with the as proposed PHQ sensor. Then, using the linear regression equations, the concentration of TNP/

Cr (VI) in the water samples was calculated. The recoveries were calculated according to Eq. (4).

$$\text{Rate of Recovery (RR, \%)} = \frac{\text{Amount of TNP/Cr(VI) found}}{\text{Amount of TNP/Cr(VI) added}} \times 100 \quad (4)$$

3.6. Effect of pH

We investigated the influence of pH on the sensing behavior of the so prepared sensing assay [55] for detection of TNP and Cr (VI). The pH was adjusted using 0.1 M NaOH and 0.1 M HCl [56] and its impact on the fluorescence detection was examined over a wide range of 4–12. As appeared in Fig. 7(a), the fluorescence intensity change in the pH range 4–10 was nearly close to each other [57]. However quenching efficiency of PHQ towards TNP detection was predominantly affected especially at very low and high pH. As the pH of the medium is close to neutral formation of electrostatic adduct between PHQ and TNP was feasible in neutral and slightly basic/acidic medium. Whereas no such complexation was feasible at extremely high/low pH [8].

In case of Cr (VI) detection, the fluorescence intensity of PHQ nanoaggregates was practically unaffected over the pH range of 4–10. In this way we construed that the as readied nanoaggregates were profoundly attractive for fluorescence detection of TNP and Cr (VI) over a wide pH extend in 95% aqueous media.

3.7. Selectivity study

To guarantee that the proposed PHQ nanoaggregates specifically recognize TNP and Cr (VI), an assortment of auxiliary analogs of TNP and metal ions were screened. Basic analogs of TNP like 1,3-dinitrobenzene, nitrobenzene, phenol, nitromethane, 2-nitrotoluene, 4-nitrophenol and 2,4-dinitrophenol were added to arrangement of PHQ nanoaggregates (Fig. 8c and d). The fluorescence emission of the sensing probe was specifically extinguished by TNP (>80%, 170 μM), while different derivatives did not demonstrated any noteworthy changes even at high concentrations. Likewise the adjustments in fluorescence profile of PHQ nanoaggregates were tried in presence of various metal ions like Hg^{2+} , Fe^{2+} , Cu^{2+} , Zn^{2+} , Cd^{2+} , Pb^{2+} , Cs^+ , Sn^{2+} , Co^{2+} , HSO_4^- , NO_3^- , CH_3COO^- , SO_4^{2-} and N_3^- (1 mM). No impressive change in fluorescence force (F_0/F) was seen in presence of any of the tried metal ion with the exception of Cr (VI) (Fig. 8a and b).

3.8. Mechanism of fluorescence quenching for TNP detection

To elucidate the possible mechanism involving detection of TNP by PHQ nanoaggregates over other nitro compounds we originally

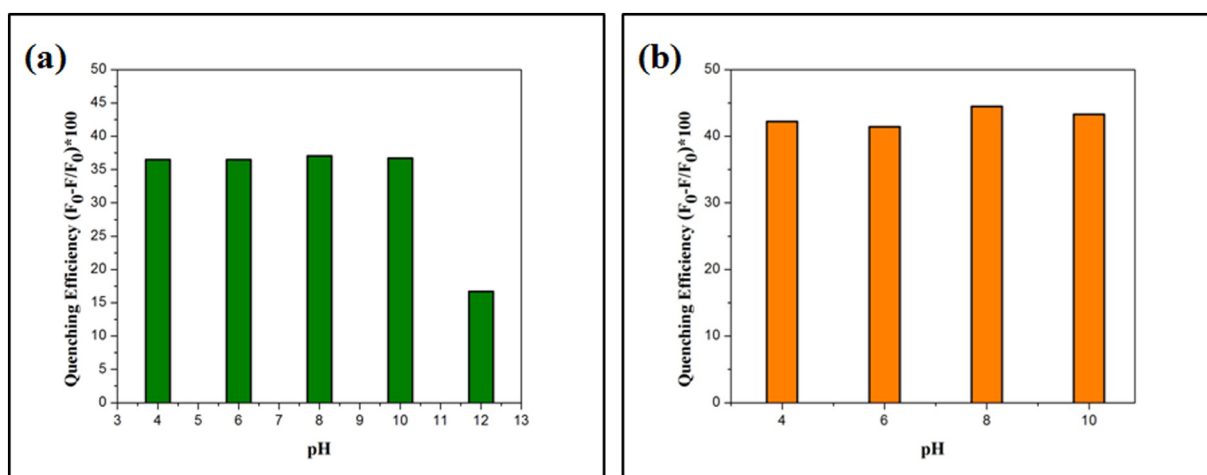


Fig. 7. Effect of pH on quenching efficiency of PHQ nanoaggregates towards detection of (a) TNP and (b) Cr (VI).

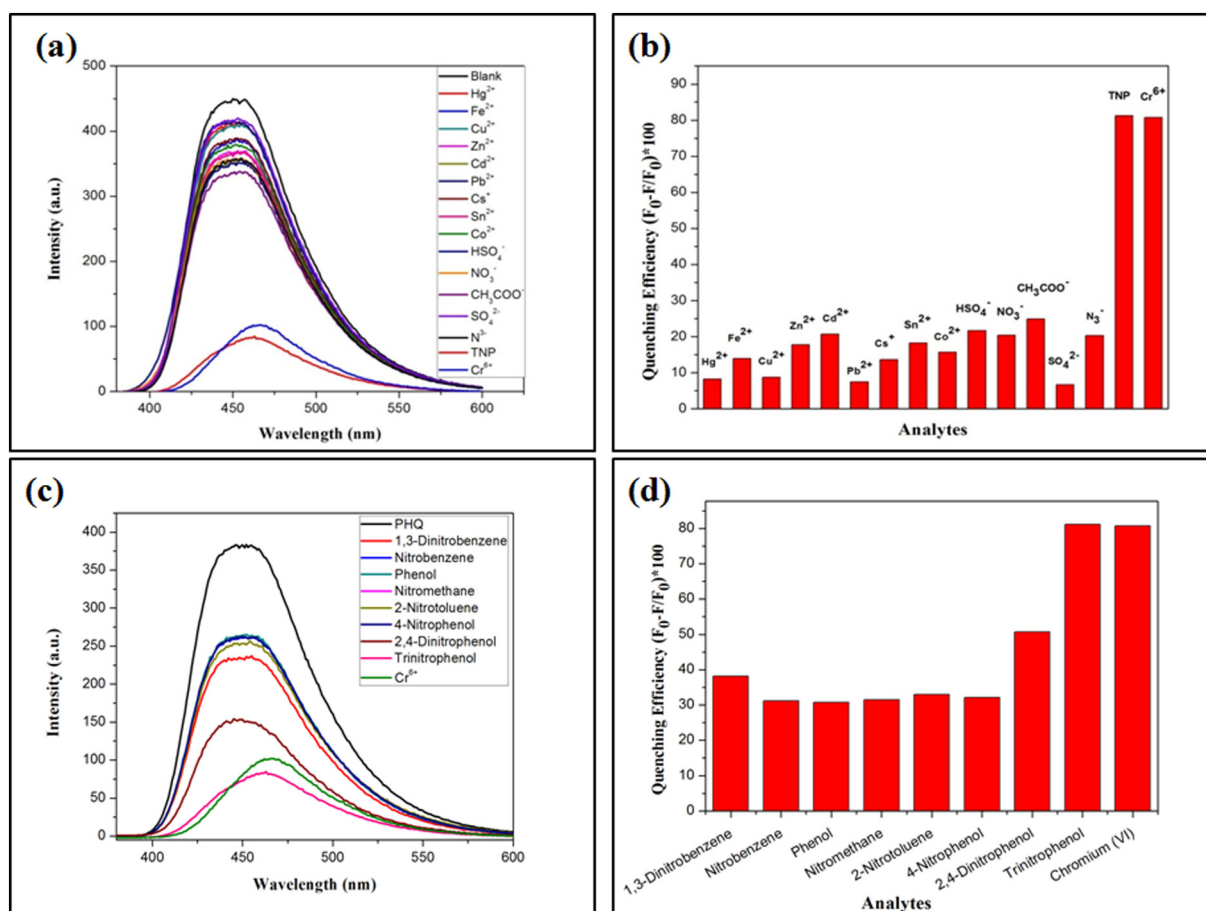


Fig. 8. Changes in fluorescence emission of PHQ nanoaggregates on addition of various (a) metal ions and (c) nitro compounds. Comparison in quenching efficiency of PHQ nanoaggregates towards various (b) metal ions and (d) nitro compounds.

investigated non-direct S-V plot (Fig. 3(b)). The deviation in linearity of S-V plot at high concentrations might be because of dynamic quenching brought about by Förster Resonance Energy Transfer (FRET). To verify this plausibility, a plot was obtained between normalized emission spectrum of PHQ and absorption spectrum of TNP and other nitro compounds (Fig. ES7). It is apparent from the plot that their existed obvious spectral overlap between absorbance spectrum of TNP and emission spectrum of PHQ in comparison with other nitro compounds. Henceforth the FRET might be the administering factor for fluorescence quenching of PHQ nanoaggregates by TNP. To further affirm dynamic quenching, fluorescence lifetime profile of PHQ in presence and absence of TNP was analyzed. As appeared in Fig. 9, fluorescence lifetime of PHQ nanoaggregates diminished in presence of TNP (100 μ M). This reduction in lifetime affirmed the presence of FRET between PHQ nanoaggregates (donor) and TNP (acceptor).

The other significant administering factor that likewise play role in recognition of TNP is photo-induced electron transfer (PET). Since TNP contains firmly acidic phenolic - OH group it has capacity to deprotonate in watery medium and exit as picrate ion. The pK_a estimations of TNP (0.38) is lowest among 2,4-dinitrophenol (4.89) and 4-nitrophenol (7.15), which record for its acidic character. Picrate ion is an electron deficient ion which can acknowledge electron from reasonable contributor. Subsequently we examined for the probability of PET from PHQ fluorophore (donor) to TNP (acceptor). PET includes electron move from LUMO of energized fluorophore to LUMO of quencher. A productive PET can happen when the LUMO of fluorophore lie somewhat above in energy then LUMO of acceptor. We determined the HOMO and LUMO energy levels of PHQ utilizing cyclic voltammetry

study (Fig. 10(a)). The value of HOMO and LUMO were -6.791 eV and -3.875 eV, respectively. As appeared in Fig. 10(b) there is plausibility of electron move from LUMO of energized PHQ to low energy LUMO of TNP. For other meddling nitro analytes, 2,4-DNP (-3.32 eV) [58], 1,3-

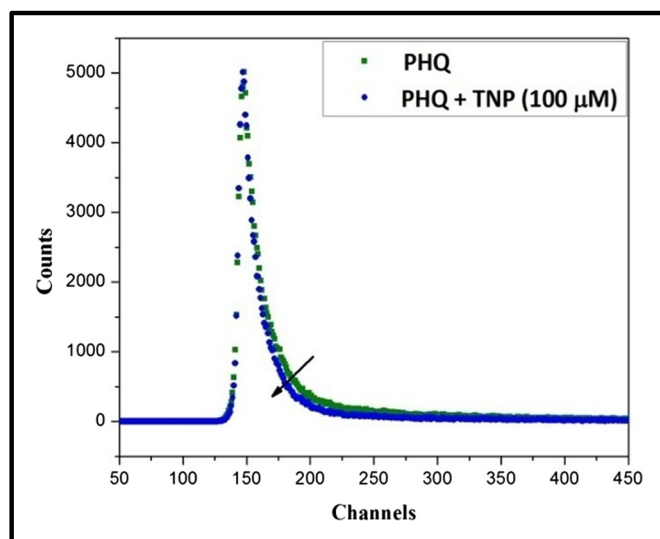


Fig. 9. Changes in fluorescence lifetime PHQ nanoaggregates in presence of TNP (100 μ M).

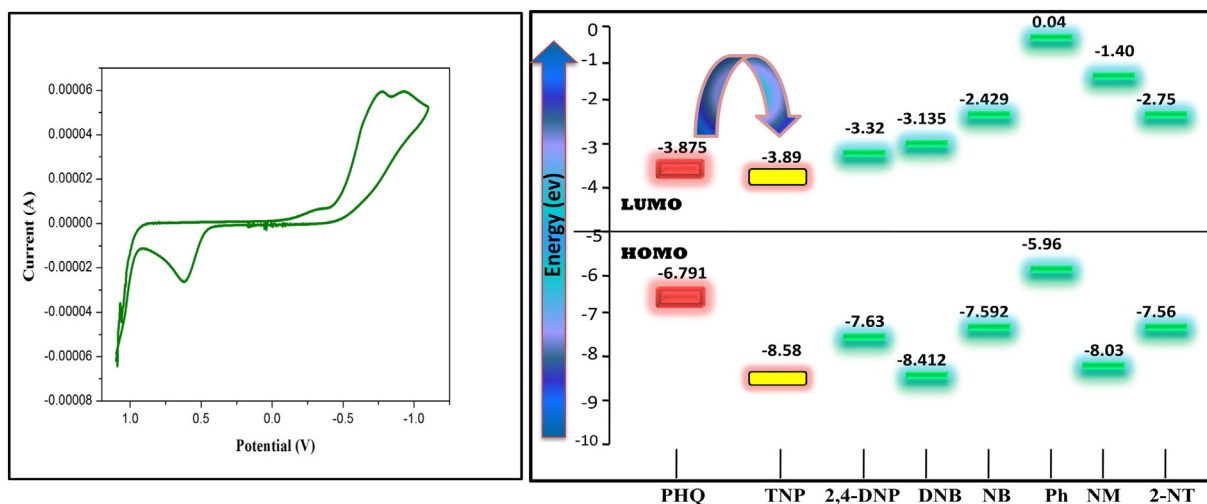


Fig. 10. (a) Cyclic voltammogram of PHQ. (b) HOMO-LUMO energy levels of PHQ and various nitro compounds.

DNB (-3.13 eV) [59], NB (-2.42 eV) [59], Ph (0.04 eV) [58], 4-NT (-2.32 eV) [60], NM (-1.90 eV) [60]; their LUMO energy levels were higher in vitality than LUMO of PHQ, thus don't participate in PET with PHQ.

Hence on the basis of above discussion, it can be concluded that sensitivity and selectivity of PHQ towards TNP is due to photo induced electron transfer and energy transfer processes.

3.9. Mechanism of fluorescence quenching for Cr (VI) detection

To decide the component for fluorescence quenching of PHQ nanoaggregates by Cr (VI) we firstly took into consideration the existence of Inner Filter Effect (IFE). IFE is a phenomenon wherein the absorption of the excitation and/or emission light of fluorophore by the quencher brings about reduction in fluorescence emission of the fluorophore. A decent spectral overlap occurs between the absorption spectra of the quencher and the excitation as well as emission spectrum of fluorophore, for productive IFE [10]. As appeared in Fig. 11, the broad absorption spectra of Cr (VI) overlap totally with excitation spectra of PHQ nanoaggregates, supporting presence of IFE. To further assure the

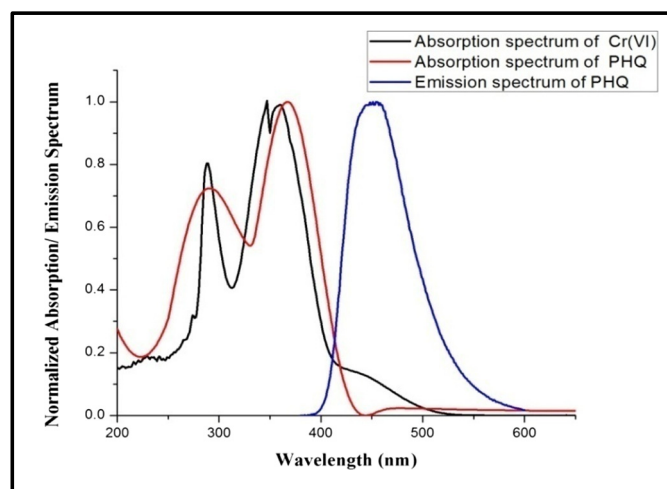


Fig. 11. Spectral overlap between absorbance spectra of Cr (VI) and excitation and/or emission spectrum of PHQ.

existence of IFE fluorescence lifetime studies were carried out, the fluorescence lifetime of PHQ in absence and presence of Cr (VI) was calculated. As shown in Fig. ES8 no prominent change in fluorescence lifetime of PHQ was observed in presence of Cr (VI) ($100 \mu\text{M}$).

The so orchestrated chemosensors for TNP and Cr (VI) recognition demonstrated practically identical or better outcomes than the strategies detailed before as appeared in Tables ES1 and ES2.

3.10. Contact mode detection

The test strip method has been proved to be an efficient method to enhance the practical application of fluorescent chemosensors [61]. The test strips covered with PHQ nanoaggregates were splendidly fluorescent under UV light. On applying $10 \mu\text{l}$ of solution of TNP/Cr (VI) (10^{-5} M), dull spot was seen on test strips, showing fluorescence quenching (Fig. 12). These spots secured a territory of 1.77 cm^2 (TNP) and 2.01 cm^2 (Cr (VI)).

3.11. Recyclability

To check the recyclability of the PHQ nanoaggregates for sensing of TNP and Cr (VI), we performed a paper strip test, wherein $10 \mu\text{l}$ of solution of TNP/Cr (VI) (10^{-5} M) was applied on the PHQ nanoaggregates test strips. To check the reversibility of test strip, we washed it with ethanol, which results in the revival of emission intensity attributing to the removal of the TNP/Cr (VI) from test strip. These experiments were repeated several times, which indicate the reusability/recyclability of these test strips for detection of TNP/Cr (VI) (Fig. ES9).

4. Conclusion

Taking everything into account, we effectively synthesized PHQ nanoaggregates that permitted dual detection of TNP and Cr (VI). Despite the fact that there are sensors revealed for recognition of TNP and Cr (VI), yet sadly there are restricted or else no report of bifunctional chemosensor for both TNP and Cr (VI). The so planned chemosensor was synthesized through one-pot simple and minimal effort approach. The PHQ derivative was effectively changed over into fluorescent nanoaggregates. The recognition of TNP and Cr (VI) were acquired at great selectivity without obstruction from different nitroaromatics and metal ions. The high values of association constant showed a decent affectability of chemosensors towards TNP and Cr (VI). The detecting measure can be adequately applied in ecological

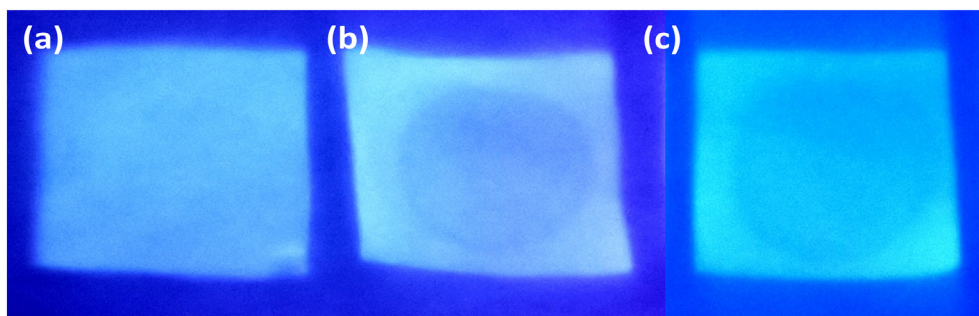


Fig. 12. Fluorescent test strips of chemosensor (a) PHQ on addition of (b) TNP and (c) Cr (VI).

chemosensing applications as appeared through the results of real sample examination. The present work can be stretched out to synthesis of new PHQ subordinates for recognition of other metal particles and nitro-explosive compounds.

CRediT authorship contribution statement

Jigyasa: Software, Methodology, Validation, Investigation, Data curation, Writing - original draft, Writing - review & editing. **Deepak Kumar:** Investigation, Data curation. **Priya Arora:** Software, Formal analysis. **Harminder Singh:** Software, Formal analysis. **Jaspreet Kaur Rajput:** Conceptualization, Methodology, Resources, Visualization, Supervision, Project administration.

Declaration of competing interest

There are no conflicts of interest to declare.

Acknowledgements

We are thankful to IIT Ropar for ESI-MS and NMR; SAIF, Cochin for HR-TEM; IIC, IIT Roorkee for FLS; SAIF, IIT-Bombay for CHN analysis; DST-FIST New Delhi, for financial assistance for acquiring the FTIR, UV-Visible and fluorescence spectrophotometer. Three of the authors (P.A, H. S, J) are thankful to MHRD, UGC, and NIT, Jalandhar, for providing the research fellowship.

Appendix A. Supplementary data

Supplementary data to this article can be found online at <https://doi.org/10.1016/j.saa.2020.118087>.

References

- [1] J. Xu, Z. Bai, F. Zu, F. Yan, J. Wei, S. Zhang, Y. Luo, A dual spectroscopic fluorescence probe based on carbon dots for detection of 2,4,6-trinitrophenol/Fe (III) ion by fluorescence and frequency doubling scattering spectra and its analytical applications, *Spectrochim. Acta Part A Mol. Biomol. Spectrosc.* 200 (2018) 150–157, <https://doi.org/10.1016/j.saa.2018.03.080>.
- [2] J. Zhang, J. Wu, G. Tang, J. Feng, F. Luo, B. Xu, C. Zhang, Multiresponsive water-stable luminescent Cd coordination polymer for detection of TNP and Cu^{2+} , *Sensors Actuators B Chem.* 272 (2018) 166–174, <https://doi.org/10.1016/j.snb.2018.05.121>.
- [3] N. Li, S.G. Liu, Y.Z. Fan, Y.J. Ju, N. Xiao, H.Q. Luo, N.B. Li, Adenosine-derived doped carbon dots: from an insight into effect of N/P co-doping on emission to highly sensitive picric acid sensing, *Anal. Chim. Acta.* 1013 (2018) 63–70, [doi:https://doi.org/10.1016/j.aca.2018.01.049](https://doi.org/10.1016/j.aca.2018.01.049).
- [4] J.C. Ni, J. Yan, L.J. Zhang, D. Shang, N. Du, S. Li, J.X. Zhao, Y. Wang, Y.H. Xing, Bifunctional fluorescent quenching detection of 2,4,6-trinitrophenol (TNP) and acetate ions via 4,4'-(9,9-dimethyl-9H-fluorene-2,7-diyl)dibenzoic acid, *Tetrahedron Lett.* 57 (2016) 4978–4982, <https://doi.org/10.1016/j.tetlet.2016.09.089>.
- [5] H. Ma, C. He, X. Li, O. Ablikim, S. Zhang, M. Zhang, A fluorescent probe for TNP detection in aqueous solution based on joint properties of intramolecular charge transfer and aggregation-induced enhanced emission, *Sensors Actuators B Chem.* 230 (2016) 746–752.
- [6] K. Duraimurugan, R. Balasaravanan, A. Siva, Electron rich triphenylamine derivatives (D- π -D) for selective sensing of picric acid in aqueous media, *Sensors Actuators B Chem.* 231 (2016) 302–312, <https://doi.org/10.1016/j.snb.2016.03.035>.
- [7] S. Mondal, P. Baire, S. Das, A.K. Nandi, Triarylamine-cored dendritic molecular gel for efficient colorimetric, fluorometric, and impedometric detection of picric acid, *Chem. – A Eur. J.* 24 (2018) 5591–5600, <https://doi.org/10.1002/chem.201705782>.
- [8] Jigyasa, J. Kaur Rajput, “On-off” novel fluorescent chemosensors based on nanoaggregates of triaryl imidazoles for superselective detection of nitro-explosive trinitrophenol in multiple solvent systems, *Sensors Actuators B Chem.* 259 (2018) 990–1005, <https://doi.org/10.1016/j.snb.2017.12.145>.
- [9] Y. Cui, M. Li, H. Wang, C. Yang, S. Meng, F. Chen, In-situ synthesis of sulfur doped carbon nitride microsphere for outstanding visible light photocatalytic Cr(VI) reduction, *Sep. Purif. Technol.* 199 (2018) 251–259, <https://doi.org/10.1016/j.seppur.2018.01.037>.
- [10] L. Zhu, X. Peng, H. Li, Y. Zhang, S. Yao, On-off-on fluorescent silicon nanoparticles for recognition of chromium(VI) and hydrogen sulfide based on the inner filter effect, *Sensors Actuators B Chem.* 238 (2017) 196–203, <https://doi.org/10.1016/j.snb.2016.07.029>.
- [11] P. Li, Y. Hong, H. Feng, S.F.Y. Li, An efficient “off-on” carbon nanoparticle-based fluorescent sensor for recognition of chromium(VI) and ascorbic acid based on the inner filter effect, *J. Mater. Chem. B.* 5 (2017) 2979–2988, <https://doi.org/10.1039/C7TB00017K>.
- [12] L. Bu, J. Peng, H. Peng, S. Liu, H. Xiao, D. Liu, Z. Pan, Y. Chen, F. Chen, Y. He, Fluorescent carbon dots for the sensitive detection of Cr(VI) in aqueous media and their application in test papers, *RSC Adv.* 6 (2016) 95469–95475, <https://doi.org/10.1039/C6RA19977A>.
- [13] S. Kang, G. Wang, H. Zhao, W. Cai, Highly efficient removal of hexavalent chromium in aqueous solutions via chemical reduction of plate-like micro/nano-structured zero valent iron, *RSC Adv.* 7 (2017) 55905–55911, <https://doi.org/10.1039/C7RA10846J>.
- [14] C. Pan, L.D. Troyer, J.G. Catalano, D.E. Giammar, Dynamics of chromium(VI) removal from drinking water by iron electrocoagulation, *Environ. Sci. Technol.* 50 (2016) 13502–13510, <https://doi.org/10.1021/acs.est.6b03637>.
- [15] R. Zhang, H. Ma, B. Wang, Removal of chromium(VI) from aqueous solutions using polyaniline doped with sulfuric acid, *Ind. Eng. Chem. Res.* 49 (2010) 9998–10,004, <https://doi.org/10.1021/ie1008794>.
- [16] G. Jian-feng, H. Chang-jun, Y. Mei, H. Dan-qun, F. Huan-bao, Ultra-sensitive fluorescence determination of chromium(VI) in aqueous solution based on selectively etching of protein-stabled gold nanoclusters, *RSC Adv.* 6 (2016) 104693–104,698, <https://doi.org/10.1039/C6RA23222A>.
- [17] K. Jin, Wei Yan, Recent Advances in Electrochemical Detection of Toxic Cr(VI), 2015 <https://doi.org/10.1039/C5RA03480A>.
- [18] L. Girard, J. Hubert, Speciation of chromium (VI) and total chromium determination in welding dust samples by flow-injection analysis coupled to atomic absorption spectrometry, *Talanta.* 43 (1996) 1965–1974, [https://doi.org/10.1016/0039-9140\(96\)01985-6](https://doi.org/10.1016/0039-9140(96)01985-6).
- [19] A. Drinčić, T. Zuliani, J. Ščančar, R. Milačič, Determination of hexavalent Cr in river sediments by speciated isotope dilution inductively coupled plasma mass spectrometry, *Sci. Total Environ.* 637–638 (2018) 1286–1294.
- [20] F. Petrucci, O. Senofonte, Determination of Cr(VI) in cosmetic products using ion chromatography with dynamic reaction cell-inductively coupled plasma-mass spectrometry (DRC-ICP-MS), *Anal. Methods.* 7 (2015) 5269–5274.
- [21] B. Umesh, R.M. Rajendran, M.T. Manoharan, Method for the determination of chromium in feed matrix by HPLC, *Poult. Sci.* 94 (2015) 2805–2815.
- [22] S. Sadeghi, A.Z. Moghaddam, A new method for separation and determination of Cr (III) and Cr(VI) in water samples by high-performance liquid chromatography based on anion exchange stationary phase of ionic liquid modified silica, *Environ. Monit. Assess.* 187 (2015), 725.
- [23] Y. Wang, W. Cao, L. Wang, Q. Zhuang, Y. Ni, Electrochemical determination of 2,4,6-trinitrophenol using a hybrid film composed of a copper-based metal organic framework and electroreduced graphene oxide, *Microchim. Acta.* 185 (2018) <https://doi.org/10.1007/s00604-018-2857-8>.
- [24] J.-H. Li, D.-Z. Kuang, Y.-L. Feng, M.-Q. Liu, S.-P. Tang, P.-H. Deng, Preparation of TNP electrochemical sensor based on silver nanoparticles/graphene oxide nanocomposite, *Chin J. Inorg. Chem.* 29 (2013) 1157–1164.

- [25] R.G. Ewing, D.A. Atkinson, G.A. Eiceman, G.J. Ewing, A critical review of ion mobility spectrometry for the detection of explosives and explosive related compounds, *Talanta*. 54 (2001) 515–529.
- [26] M. López-López, C. García-Ruiz, Infrared and Raman spectroscopy techniques applied to identification of explosives, *TrAC Trends Anal. Chem.* 54 (2014) 36–44.
- [27] Y. Ma, S. Huang, M. Deng, L. Wang, White upconversion luminescence nanocrystals for the simultaneous and selective detection of 2,4,6-trinitrotoluene and 2,4,6-trinitrophenol, *ACS Appl. Mater. Interfaces*. 6 (2014) 7790–7796, <https://doi.org/10.1021/am501053n>.
- [28] H. Wang, S. Liu, Y. Xie, J. Bi, Y. Li, Y. Song, S. Cheng, D. Li, M. Tan, Facile one-step synthesis of highly luminescent N-doped carbon dots as an efficient fluorescent probe for chromium(VI) detection based on the inner filter effect, *New J. Chem.* 42 (2018) 3729–3735, <https://doi.org/10.1039/C8NJ00216A>.
- [29] S. Bhatt, M. Bhatt, A. Kumar, G. Vyas, T. Gajaria, P. Paul, Green route for synthesis of multifunctional fluorescent carbon dots from Tulsi leaves and its application as Cr (VI) sensors, bio-imaging and patterning agents, *Colloids Surfaces B Biointerfaces*. 167 (2018) 126–133, <https://doi.org/10.1016/j.colsurfb.2018.04.008>.
- [30] N. Tripathi, S. Sandhu, P. Singh, A. Mahajan, M. Kaur, S. Kumar, Dansyl conjugated tripodal AIEEgen for highly selective detection of 2,4,6-trinitrophenol in water and solid state, *Sensors Actuators B Chem.* 231 (2016) 79–87, <https://doi.org/10.1016/j.snb.2016.03.008>.
- [31] FLIR Fido NXT Maintenance Management, Support, Repair – KD Analytical, (n.d.). <http://www.kdanalytical.com/instruments/flir-fido-nxt.aspx>.
- [32] Fido® XT Explosives Detector | FLIR Systems, Inc. | MRIGlobal CBRNE Tech Index, (n.d.). <http://www.cbrnetechindex.com/p/4270/FLIR-Systems-Inc/Fido-XT-Explosives-Detector>.
- [33] N. Rahbar, Z. Salehnezhad, A. Hatamie, A. Babapour, Graphitic carbon nitride nanosheets as a fluorescent probe for chromium speciation, *Microchim. Acta*. 185 (2018), 101. <https://doi.org/10.1007/s00604-017-2615-3>.
- [34] C. Zhang, S. Zhang, Y. Yan, F. Xia, A. Huang, Y. Xian, Highly fluorescent polyimide covalent organic nanosheets as sensing probes for the detection of 2,4,6-trinitrophenol, *ACS Appl. Mater. Interfaces*. 9 (2017) 13415–13421, <https://doi.org/10.1021/acsmi.6b16423>.
- [35] L. Wang, M. Cui, H. Tang, D. Cao, Fluorescent Nanoaggregates of Quinoxaline Derivatives for Highly Efficient and Selective Sensing of Trace Picric Acid, 2018 <https://doi.org/10.1016/j.dyepig.2018.03.036>.
- [36] B. Xu, X. Wu, H. Li, H. tong, L. Wang, Selective detection of TNT and picric acid by conjugated polymer film sensors with donor–acceptor architecture, *Macromolecules*. 44 (2011) 5089–5092, <https://doi.org/10.1021/ma201003f>.
- [37] B.B. Campos, M. Algarra, B. Alonso, C.M. Casado, J. Jiménez-Jiménez, E. Rodríguez-Castellón, J.C.G. Esteves da Silva, Fluorescent sensor for Cr(VI) based in functionalized silicon quantum dots with dendrimers, *Talanta*. 144 (2015) 862–867, <https://doi.org/10.1016/j.talanta.2015.07.038>.
- [38] H.-Y. Li, D. Li, Y. Guo, Y. Yang, W. Wei, B. Xie, On-site chemosensing and quantification of Cr(VI) in industrial wastewater using one-step synthesized fluorescent carbon quantum dots, *Sensors Actuators B Chem.* 277 (2018) 30–38, <https://doi.org/10.1016/j.snb.2018.08.157>.
- [39] Y.-X. Shi, F.-L. Hu, W.-H. Zhang, J.-P. Lang, A unique Zn(II)-based MOF fluorescent probe for the dual detection of nitroaromatics and ketones in water, *CrystEngComm*. 17 (2015) 9404–9412, <https://doi.org/10.1039/C5CE02000J>.
- [40] J. Dong, H. Xu, S.-L. Hou, Z.-L. Wu, B. Zhao, Metal–organic frameworks with Tb4 clusters as nodes: luminescent detection of chromium(VI) and chemical fixation of CO₂, *Inorg. Chem.* 56 (2017) 6244–6250. doi:<https://doi.org/10.1021/acs.inorgchem.7b00323>.
- [41] S. Kumari, S. Joshi, T.C. Cordova-Sintjago, D.D. Pant, R. Sakhuja, Highly sensitive fluorescent imidazolium-based sensors for nanomolar detection of explosive picric acid in aqueous medium, *Sensors Actuators B Chem.* 229 (2016) 599–608.
- [42] Y. Zhang, H. Li, G. Zhang, X. Xu, L. Kong, X. Tao, Y. Tian, J. Yang, Aggregation-induced emission enhancement and mechanofluorochromic properties of α -cyanostilbene functionalized tetraphenyl imidazole derivatives, *J. Mater. Chem. C*. 4 (2016) 2971–2978, <https://doi.org/10.1039/C5TC03348A>.
- [43] V. Bhalla, A. Gupta, M. Kumar, Fluorescent nanoaggregates of pentacenequinone derivative for selective sensing of picric acid in aqueous media, *Org. Lett.* 14 (2012) 3112–3115.
- [44] H.-H. Lin, Y.-C. Chan, J.-W. Chen, C.-C. Chang, Aggregation-induced emission enhancement characteristics of naphthalimide derivatives and their applications in cell imaging, *J. Mater. Chem.* 21 (2011) 3170–3177, <https://doi.org/10.1039/C0JM02942D>.
- [45] Q. Li, Y. Qian, Aggregation-induced emission enhancement and cell imaging of a novel (carbazol-N-yl)triphenylamine–BODIPY, *New J. Chem.* 40 (2016) 7095–7101, <https://doi.org/10.1039/C6NJ01495J>.
- [46] S. Phukan, M. Saha, A.K. Pal, S. mitra, Synthesis and fluorescence behavior of photoactive polyhydroquinoline derivatives: a combined experimental and DFT study, *J. Mol. Struct.* 1039 (2013) 119–129, <https://doi.org/10.1016/j.molstruc.2013.02.004>.
- [47] P. Deng, L. Liu, S. Ren, H. Li, Q. Zhang, N-acylation: an effective method for reducing the LUMO energy levels of conjugated polymers containing five-membered lactam units, *Chem. Commun.* 48 (2012) 6960–6962.
- [48] A. Kalita, N.V.V. Subbarao, P.K. Iyer, Large-scale molecular packing and morphology-dependent high performance organic field-effect transistor by symmetrical naphthalene diimide appended with methyl cyclohexane, *J. Phys. Chem. C* 119 (2015) 12772–12779.
- [49] S. Hussain, A.H. Malik, M.A. Afroz, P.K. Iyer, Ultrasensitive detection of nitroexplosive – picric acid via a conjugated polyelectrolyte in aqueous media and solid support, *Chem. Commun.* 51 (2015) 7207–7210.
- [50] K. Sharma nee Kamaldeep, S. Kaur, V. Bhalla, M. Kumar, A. Gupta, Pentacenequinone derivatives for preparation of gold nanoparticles: facile synthesis and catalytic application, *J. Mater. Chem. A*. 2 (2014) 8369–8375.
- [51] M. Shyamal, S. Maity, A. Maity, R. Maity, S. Roy, A. Misra, Aggregation induced emission based “turn-off” fluorescent chemosensor for selective and swift sensing of mercury (II) ions in water, *Sensors Actuators B Chem.* 263 (2018) 347–359.
- [52] Y. Ren, J.W.Y. Lam, Y. Dong, B.Z. Tang, K.S. Wong, Enhanced emission efficiency and excited state lifetime due to restricted intramolecular motion in silole aggregates, *J. Phys. Chem. B*. 109 (2005) 1135–1140.
- [53] Y. Deng, W. Yuan, Z. Jia, G. Liu, H- and J-aggregation of fluorene-based chromophores, *J. Phys. Chem. B*. 118 (2014) 14536–14545.
- [54] M. Mās-Montoya, R.A.J. Janssen, The effect of H- and J-aggregation on the photophysical and photovoltaic properties of small thiophene–pyridine–DPP molecules for bulk-heterojunction solar cells, *Adv. Funct. Mater.* 27 (2017), 1605779.
- [55] J.K. Rajput Jigyasa, Bio-polyphenols promoted green synthesis of silver nanoparticles for facile and ultra-sensitive colorimetric detection of melamine in milk, *Biosens. Bioelectron.* 120 (2018) 153–159, <https://doi.org/10.1016/j.bios.2018.08.054>.
- [56] S. Kasthuri, P. Gawas, S. Maji, N. Veeraiiah, N. Venkatramaiah, Selective detection of trinitrophenol by amphiphilic dimethylaminopyridine-appended Zn(II)phthalocyanines at the near-infrared region, *ACS Omega*. 4 (2019) 6218–6228, <https://doi.org/10.1021/acsomega.8b02394>.
- [57] L. Lin, M. Rong, S. Lu, X. Song, Y. Zhong, J. Yan, Y. Wang, X. Chen, A facile synthesis of highly luminescent nitrogen-doped graphene quantum dots for the detection of 2,4,6-trinitrophenol in aqueous solution, *Nanoscale*. 7 (2015) 1872–1878.
- [58] J.H. Ko, J.H. Moon, N. Kang, J.H. Park, H.-W. Shin, N. Park, S. Kang, S.M. Lee, H.J. Kim, T.K. Ahn, J.Y. Lee, S.U. Son, Engineering of Sn-porphyrin networks on the silica surface: sensing of nitrophenols in water, *Chem. Commun.* 51 (2015) 8781–8784.
- [59] M. SK, S. Biswas, A thiadiazole-functionalized Zr(IV)-based metal-organic framework as a highly fluorescent probe for the selective detection of picric acid, *CrystEngComm*. 18 (2016) 3104–3113.
- [60] X. Sun, X. Ma, C.V. Kumar, Y. Lei, Protein-based sensitive, selective and rapid fluorescence detection of picric acid in aqueous media, *Anal. Methods*. 6 (2014) 8464–8468.
- [61] L. Bai, Y. Xu, G. Li, S. Tian, L. Li, F. Tao, A. Deng, S. Wang, L. Wang, A highly selective turn-on and reversible fluorescent chemosensor for Al³⁺ detection based on novel silylidene Schiff base-terminated PEG in pure aqueous solution, *Polymers (Basel)*. 11 (2019) 573.